Uncovering High-Dimensional Visual Neural Structures: A Topological Approach to Representational Similarity Analysis

Coco Wang; Reza D. Farivar
Cognitive Science Program, McGill University Department of Ophthalmology and Visual Science, McGill University

Abstract

Representational Similarity Analysis (RSA) is widely used to study neural representations but fails to capture non-linear, high-dimensional structures in complex neural data. Its reliance on linear metrics risks false equivalences between topologically distinct computational systems. Representational Topology Analysis (RTA) addresses this limitation by using persistence diagrams to detect topological features like clusters, loops, and voids. While early RTA results have shown promise against RSA, previous applications of RTA were applied on datasets with a limited scale of subjects and conditions. This study implements RTA on the Natural Scene Dataset (NSD) using the TDApplied R package as well as the tdads pipeline in Python. By analyzing 30,000 conditions across 40 trials and comparing results with RSA, we argue that only through such large-scale application can we fully reveal RTA's strengths —and its constraints.

INTRODUCTION

Representational Similarity Analysis (RSA) has become a central method in systems neuroscience for comparing activity patterns across brain regions (Kriegeskorte, Mur, & Bandettini, 2008). Unlike frameworks that focus on modelling the computational models of individual neurons (David & Gallant, 2005) (Koch, 1999) (Rieke, Warland, De Ruyter van Steveninck, & Bialek, 1999), RSA offers a scalable method for analyzing neural data by abstracting activity patterns into representational dissimilarity matrices (RDMs). These matrices compare neural responses across experimental conditions and allow researchers to quantify the structure of neural representations using second-order isomorphism (Shepard & Chipman, 1970), without requiring neuron-to-neuron correspondence.

This abstraction has led to notable advances. For instance, Drucker and Aguirre 2009 (Drucker & Aguirre, 2009) used RSA to uncover distinct spatial scales of neural representation in the lateral and ventral occipital complex (LOC). In a large-scale study involving over 30,000 natural scene images, Allen et al.(Allen, St-Yves, Wu, & al., 2022) employed RSA as a core tool to probe the structure of visual representations across the brain. They found that activity patterns are highly correlated among faces, but this phenomenon is to a lesser degree among animals. These studies demonstrate RSA's flexibility and power in uncovering meaningful patterns at the population level.

However, what's not discussed and scrutinized frequently is that RSA's strengths come with critical limitations. Among the various dissimilarity metrics used to construct RDMs (Kriegeskorte, Mur, & Bandettini, 2008), correlation distance (1-Pearson) is frequently favoured due to its normalization for mean activation and spatial variability. Yet this preference is often asserted without rigorous quantitative validation. More critically, RSA's reliance on linear similarity measures can obscure true structures of high-dimensional neural data (Dujmović, Bowers, Adolfi, & Malhotra, 2022), (Chen, Martin, & Fischer-Baum, 2021). Brown and Reza argued that two computational systems might appear similar through RSA yet differ fundamentally in the mechanisms generating those patterns (Brown & Farivar, 2024). Singh et al had argued that the topological structure of activity patterns in V1 when the cortex is spontaneously active is consistent with the topology of a sphere (Singh & al., 2008). A similar property was discovered in Curto's research about topology and its underlying neural code. He found that

the hexagonal domain of the spiking activity of rats' grid cells is "precisely a torus" (Curto, 2016). RSA, by reducing high-dimensional relationships into pairwise distances, fails to capture such critical topological properties (Fig. 1).

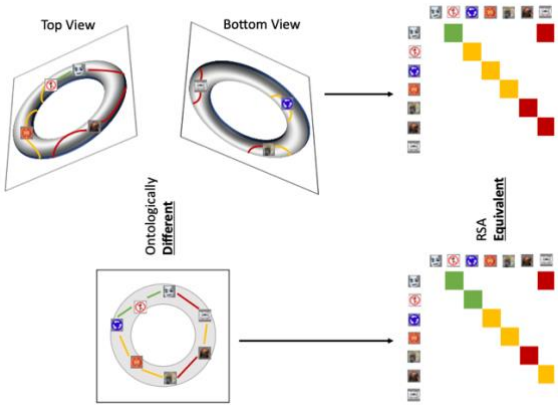

Fig. 1 | Sampled representations from a torus, projected onto an annulus, and the resulting two RDMs. The two RDMs would be considered equivalent by RSA, despite distinct topological spaces (11)

To address these shortcomings, high-dimensional shape structures of the dataset must be accounted for. Brown and Farivar introduced Representational Topology Analysis (RTA), a method that goes beyond spatial correlation and characterizes the shape of neural representations. By incorporating Persistent Diagrams (PDs) – a tool to identify "long-lived" topological features in the dataset – RTA captures important data structures such as clusters (H0), loops (H1), and voids (H2). This leads to a fundamentally different type of second-order isomorphism: one grounded in the PD comparison of representational space rather than pairwise similarity. More importantly, RTA is said to be robust to noise (Edelsbrunner, Letscher, & Zomorodian, 2002) and invariant to data point ordering. As the datasets grow, the topological features can eventually converge (Chazal, Glisse, Labruère, & Michel, 2014) to underlying structural properties.

Despite all these promises, RTA remains under-tested. The two datasets used in Brown and Farivar's study offer limited generalizability: one includes average RDMs from only a handful of human and monkey inferior temporal (IT) cortex responses to 92 visual stimuli (Kriegeskorte N. , et al., 2008), and the other analyzes task-free naturalistic stimuli from only 27 subsamples of 53 subject pairs (Zhang & Farivar, 2020). These constraints raise doubts about RTA's reliability in detecting meaningful topological structures in more complex or variable datasets. In the first study, the resulting Vietoris-Rips graph primarily revealed a binary animate–inanimate division. While this aligns well with established object representations in the IT cortex, the emergence of only a few domain axes (e.g. animacy) suggests a potential limitation. It remains unclear whether this categorization reflects an intrinsic tendency of RTA to oversimplify representational geometry or merely a consequence of limited stimulus diversity and sample size. In the meantime, the task-free paradigm used in the second study comes at the cost of interpretability. Without stimulus-specific tasks, it becomes difficult to anchor the resulting topologies to specific cognitive or semantic dimensions.

Without rigorous testing on larger and more diverse datasets, RTA's advantages over RSA remain speculative. The Natural Scene Dataset (NSD) provides an ideal opportunity to confront this challenge. With over 73,000 image stimuli, high spatial resolution, and repeated presentations of roughly 30,000 images per 8 subjects (Allen, St-Yves, Wu, & al., 2022), NSD offers a robust and replicable testbed for assessing RTA's effectiveness. We argue that only by applying RTA methodologies to such a large and information-rich dataset can we evaluate its true capacity to reveal meaningful topological features. By a direct comparison between the results of RTA and

previous RSA studies on the NSD (e.g. Allen et al.), we can illuminate the strength and potential – or perhaps limitations – of RTA with better validity.

To pursue this goal, I applied RTA to the neural data of the first subject in the NSD experiment. Seven regions of interest (ROI) are being examined closely: Primary Visual Cortex (V1), Second Visual Area (V2), Third Visual Area (V3), Fourth Visual Area (V4), Eighth Visual Area (V8), Area Lateral Occipital 2 (Lo2), and Posterior-Infero-Temporal Complex (PIT). These ROIs span early to mid-level visual processing stages, offering a diverse landscape for evaluating RTA. Detailed definitions of each ROI can be found in the HCP-MMP1 atlas online document (Atlases — neuroimaging core 0.1.1 documentation. (n.d.).).

METHODS

Subjects

This study utilized the Natural Scenes Dataset (NSD), a publicly available dataset that includes high-resolution (1.8-mm) whole-brain 7T functional magnetic resonance imaging (fMRI) data from eight carefully screened human participants. Each subject viewed approximately 9,000–10,000 unique natural scene images throughout 30–40 scan sessions distributed across one year. Across all participants, NSD encompasses responses to 70,566 distinct natural scene images, making it an order of magnitude larger than similar fMRI datasets ever used in RTA.

Each participant viewed 750 natural scene images per session while completing a cognitive task. Specifically, participants were asked to judge whether each image had been presented at any point in the past while maintaining central fixation. The dataset also includes extensive metadata, such as trial-wise behavioural responses and fixation stability, enabling a comprehensive analysis of neural responses to naturalistic visual stimuli. More details on the dataset can be found at https://naturalscenesdataset.org/.

Experimental Design

Trial Design. During each trial, participants maintained central fixation while being presented with a sequence of colour natural scenes in a 3-s ON/1-s OFF trial structure. Their task was to determine whether each image had been previously shown at any point in the study. The stimuli were sourced from Microsoft's COCO14 dataset, which includes detailed object annotations.

Run and Session Structure. Each experimental run lasted approximately 5 minutes and comprised 62 or 63 stimulus trials, interspersed with occasional blank trials to provide baseline measurements. A single scan session consisted of 12 such runs, totalling 750 stimulus trials per session. The experimental timeline included an initial screening session, 30–40 NSD core sessions, and two concluding sessions dedicated to synthetic image and mental imagery processing (nsdsynthetic and nsdimagery). The first NSD core session was designated as day 0 for each participant. By the end of the experiment, each subject will view up to 30,000 NSD images.

Behavioural Performance. To quantify participants' performance, their responses were categorized into three trial types, with the percentage of trials in which an 'old' response was given recorded and analyzed for accuracy.

Stimulus. The stimuli used in this study consisted of natural scene images sourced from the Natural Scenes Dataset. Each image was taken from the Microsoft COCO14 dataset, which includes extensive object annotations, allowing for detailed analyses of visual features. The selection of stimuli ensured a wide variety of scene compositions, promoting robust neural responses across experimental conditions.

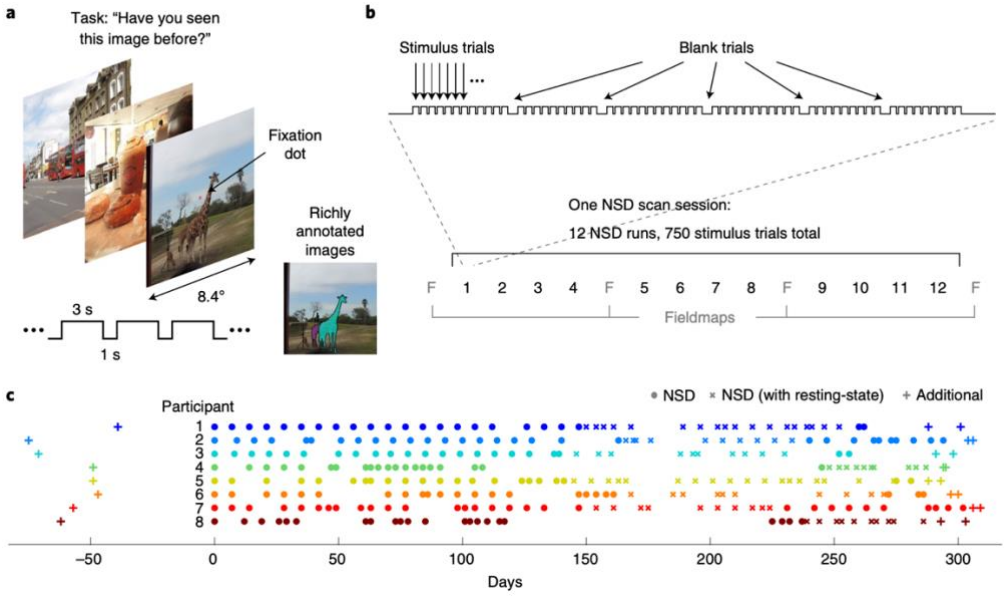

Fig. 2 | Design of the NSD experiment. a, Trial design **b,** Run and session design. **c,** Timeline of 7T fMRI scan sessions. (Kriegeskorte, Mur, & Bandettini, 2008)

Equipment and Material

All data processing and analysis were conducted using two primary computing environments:

- Apple MacBook Pro (Apple M3 Pro, macOS 15.3.1): Used for initial data inspection, ROI mapping, and smaller-scale computations.
- Dell XPS 8960 (Windows 11 Home, Intel Core i7-13700, 32 GB RAM for RSA; 64 GB RAM for RTA): Employed for high-memory, large-scale computations such as full-session RDM construction (e.g., 30,000 × 30,000 matrices).
- WSL Linux environment for RTA

The following software tools were used:

- Python (nibabel, numpy, matplotlib, pandas, PyDory, tdads): Automated Representational Dissimilarity Matrix (RDM) construction and general data processing.
- Azure Data Studio: Efficient filtering and exploration of large-scale beta value matrices.
- R (TDApplied package): Applied for Topological Data Analysis (TDA) to capture high-dimensional structural patterns (Brown & Farivar, 2025).
- AFNI & Freeview: Used for visualization and anatomical localization of regions of interest (ROIs).

- Amazon Web Services (AWS) S3: Paired with awscli for recursive download of data.

Task

In this study, we aimed to perform a Representational Similarity Analysis (RSA) and subsequently apply a Representational Topology Analysis (Brown & Farivar, 2025) on the full 40 sessions of subject 1 from the NSD experiment, involving 30,000 image stimuli in total. The workflow consisted of several key steps, as outlined below.

Representational Similarity Analysis (RSA). We performed RSA on data across all 40 sessions of subject 1 in the NSD (Natural Scenes Dataset) experiment. The fMRI beta values were surface-based and aligned to the fsaverage cortical surface, with each vertex (node) representing the beta value (strength and direction of neural response to the specific stimulus) across different image conditions. The data of each of the 40 sessions was stored in .mgh format, totalling 163,842 cortical vertices each.

To assign each vertex to a specific region of interest (ROI), we utilized the HCP_MMP1.mgz atlas and its corresponding label file, HCP_MMP1.mgz.txt. This allowed us to map each of the 163,842 cortical nodes to one of 180 predefined brain regions. The ROI assignments were integrated into our data matrix, enabling us to analyze region-specific activation patterns.

Once the node-to-ROI mapping was established, we constructed ROI-specific activity patterns by extracting beta values from each session and concatenated them across all 40 sessions for each ROI. This is made possible by the continuous nature of the NSD experiment (30,000 continuous trials divided into 40 sessions for each subject). This yielded a single, comprehensive activity matrix per ROI, with rows corresponding to each of the 163,842 nodes and columns to each of the 30,000 experimental conditions (images). We focused on seven visual areas: V1, V2, V3, V4, V8, Lo2, and PIT.

For each ROI, we computed a **representational dissimilarity matrix (RDM)** using Spearman correlation distance (1 – Spearman correlation) across 30,000 image conditions. This resulted in seven RDMs (one per ROI), capturing the representational structure of neural activity within each visual region.

To compare representations across ROIs, we performed the RSA by calculating Spearman correlations between the upper triangular values of each RDM. These results were visualized in a heatmap, illustrating the degree of representational similarity between brain regions (fig. 3). The activity patterns appear to be highly similar between early visual areas like V1, V2, V3 and V4, but to a lesser degree in higher visual areas. This aligns with the progressive nature of visual information processing in the brain. Early areas share more structured and image-driven encoding, while higher areas branch into more specialized, semantically enriched spaces (Yamins & DiCarlo, 2016).

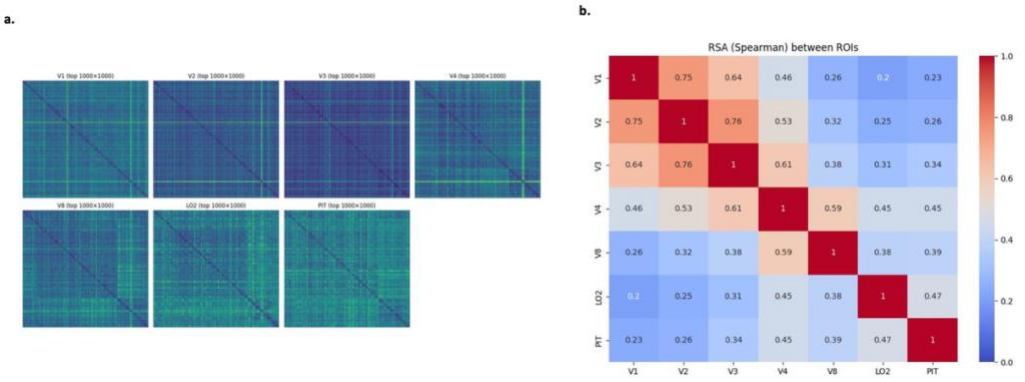

Fig. 3 | Representational Similarity Analysis (RSA). a, the top 1000 x 1000 representational dissimilarity matrices (RDM) of seven selected regions of interest **b,** second-order isomorphism of RDMs calculated using Spearman correlation distance

While RSA offers a useful atlas of representational similarity across brain regions, its summarization of high-dimensional neural data imposes a critical limitation. With over 30,000 distinct NSD image stimuli, collapsing each region's internal structure into a scalar matrix risks obscuring meaningful sub-patterns—such as category-specific clusters, semantic gradients, or representational asymmetries. This reductionist view may overlook how different regions encode unique aspects of the stimulus space. To better preserve and explore important topological structures of neural representations, we turn to Representational Topology Analysis (RTA), which offers a more expressive lens on the topology of complex neural data.

Representational Topology Analysis (RTA)

To uncover higher-order structural patterns in fMRI data, I employed Topological Data Analysis using TDApplied. The approach was applied again to the 7 RDMS calculated from early and higher visual areas (e.g., V1, V2, V3, V4, LO2, PIT), aiming to uncover topological features such as loops (1-dimensional homology, h1) that may reveal latent structures and stimulus relationships not captured by RSA.

Persistent homology over 40 trials (30,000 stimuli)

Due to RAM limitations and the scale of the data, several preprocessing steps were applied to each RDM before the topological analysis. The original RDMs were first thresholded into edge lists using cutoff values derived from the enclosing_radius function in tdads (Brown & al., 2024), a Python-based adaptation of the R package TDApplied. To further reduce memory footprint, data precision was downgraded to float32, and the enclosing radius threshold was lowered from 70% to 50%. These optimizations reduced the RDM size from 8.76 GB to 3.7 GB for V1.

For computing persistent homology and representative cycles, we used PyDory (Nihcompmed.) instead of Ripser, as it offers better scalability and computational efficiency on large datasets. However, PyDory outputs raw birth-death value files with thousands of persistent features, making visualization and interpretation of persistence diagrams challenging within the current Python pipeline.

To proceed and evaluate RTA's performance on the NSD dataset, we reduced the dataset size and focused on implementing the full RTA pipeline on a single trial from subject 1 as a first step.

Persistent homology of a single trial (750 stimuli)

RDM for each of the seven regions of interest is recalculated across 750 stimuli of a single trial of subject 1 using the same procedure above.

Each region's RDM was then subjected to bootstrapping via the TDApplied R package *bootstrap_persistence_thresholds function* (Brown & Farivar, 2025) to identify statistically significant persistent features. This method involves repeated random sampling of the RDM to generate a null distribution of persistence diagrams, allowing for empirical p-value estimation. In this study, we are only considering two dimensions (maxdim = 1) and keeping features in the top 2.5% of the null distribution (thresh = 2).

Due to the random nature of bootstrapping, results varied slightly between runs. I applied 10 runs to each ROI on average. However, consistent trends emerged:

- **V1** consistently yielded 4 to 6 significant loop features. One example output is shown in Fig. 4.
- **V2** and **V3** often exhibited 1 to 2 features.
- **V4, V8, LO2,** and **PIT** generally lacked significant features across runs, suggesting a lower level of topological structure in their RDMs.

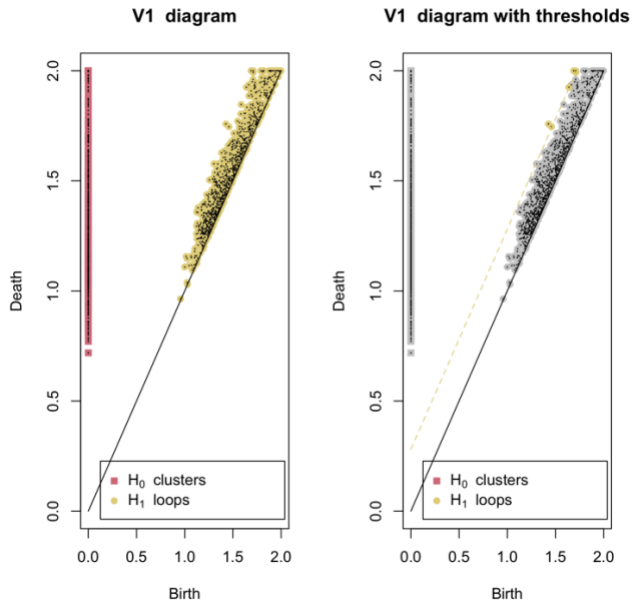

Fig. 4 | Persistent Diagram (PD) of RDM of V1. This plot shows that six significant H1 features are found.

Mapping Features to Stimuli

For each detected loop, we extracted the underlying trials from the subsetted_representatives output of the bootstrapping method. In the NSD experiments, image stimuli are presented and repeated in a specific pattern. In the Natural Scenes Dataset (NSD), each of the 10,000 images was shown three times across 30,000 trials, with a fixed trial ordering shared across participants (Allen, St-Yves, Wu, & al., 2022). The first 1,000 image slots were reserved for a shared set ("shared1000"), while the remaining 9,000 were unique per participant. To control repetition timing and ensure balanced memory difficulty, image presentations were scheduled using a circular sampling procedure. For each image, a mixture of a von Mises distribution (60%)

and a uniform distribution (40%) was used to determine three repetition times, with the von Mises peak randomly placed on a conceptual circle. This circular trial layout was then unwrapped into a linear sequence, split evenly into 40 scanning sessions (750 trials/session), ensuring a uniform distribution of repetitions and minimizing clustering effects across the experiment.

According to the ordering, we matched each trial to the image stimulus via a trial-to-nsdID mapping. This allowed visual inspection of the actual stimuli contributing to each topological feature (Fig. 5).

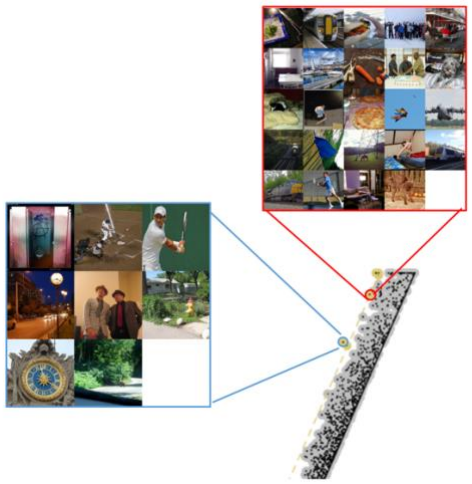

Fig. 5 | Trial-to-nsdID mapping. This plot zooms in on two significant H1 features (out of six) of V1. Their underlying trials and corresponding NSD images are displayed.

Vietoris-Rips (VR) Graph Construction and Visualization

To visualize the structure of each feature, I used the Vietoris–Rips graph method (*vr_graphs()*), which constructs a VR graph from the filtered RDM of interest (Method 1). VR graphs provide an intuitive, geometric view of the similarity structure encoded in the RDM, highlighting clusters, transitions, and loops, which correspond to topological features revealed through persistent homology. By filtering the original RDM to include only the trials forming a significant loop, I generated a reduced distance matrix that preserves only the relevant stimulus relationships. Then, using *plot_vr_graph()*, I rendered the graph with node colours corresponding to different features and overlaid each node with its corresponding image stimulus using *rasterImage()*.

I explored an alternative approach (Method 2) where the full VR graph was constructed first, and then subgraphs corresponding to specific features were extracted. However, this method proved more limited due to constraints in plot_vr_graph(), which expects an object directly from vr_graphs(). Therefore, Method 1 was preferred for flexibility and interpretability.

Observations and Interpretation

The resulting VR graphs offered an interpretable, geometric visualization of stimulus clusters forming topological loops (fig. 6). However, there are several things to note: not all features detected using bootstrapping are valid, and some of the features vary across different funs of bootstrapping. The first phenomenon happens when the persistence diagram shows a loop, but the representative cycle cannot be reliably reconstructed. At the same time, some cycles might be borderline significant and may show up

differently across runs — they could have meaningful persistence values but ambiguous or unstable representatives.

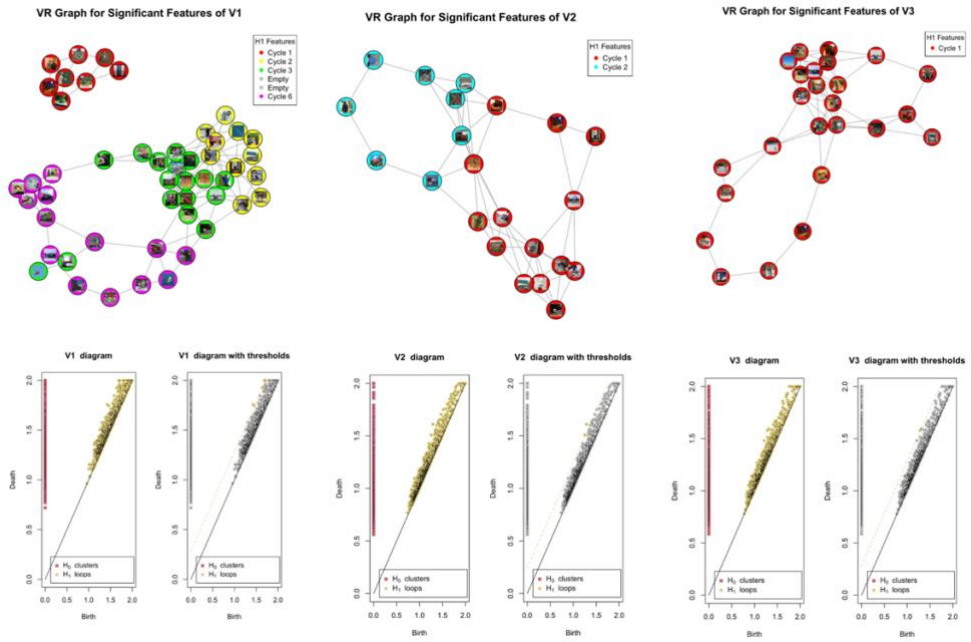

Fig. 6 | Vietoris-Rips (VR) Graph for significant features in V1 to V3 and corresponding PDs. Some cycles have empty nodes and are not real topological features with valid representative cycles.

In the VR graph of the primary visual cortex (V1), one of the topological features—Feature 1—was distinctly separated from the rest. While these images in Feature 1 do not form an obvious semantic or categorical group, they exhibit prominent vertical edges, elongated high-contrast structures, or distinct spatial frequency patterns—such as the edges of the door or the sharp contrast lines of sports equipment and poles. Given that V1 neurons are highly sensitive to line orientation, especially vertical and diagonal edges, and respond selectively to spatial frequency and edge direction, the grouping of these visually distinct images into a single feature might suggest a shared activation pattern for vertical lines across V1's early visual detectors.

In contrast, the VR graph of the third visual area (V3) revealed a single, prominent topological feature shaped like a figure "8," composed of two interconnected loops. Notably, one of these loops clustered animal-related stimuli more tightly than observed in earlier visual areas like V1 or V2. This emerging structure suggests a potential transition from low-level visual representations (e.g., edges, textures, symmetry) toward mid-level or even proto-semantic groupings. Although V3 is still considered part of the early visual cortex, it is associated with the processing of global shapes and motion and hence may begin to reflect more integrated representations of visual scenes.

In higher-order regions—including V4, V8, LO2, and PIT—no statistically significant topological features were consistently detected. This resembles RSA's conclusion of these regions being less correlated overall. However, it is important to note that the current analysis is solely based on a single session from the first participant in the NSD experiment, encompassing only 750 image stimuli and responses in total. Due to greater response variability and abstract coding in higher-order areas like LO2 and PIT, it is likely that more

robust, stable topological patterns would emerge with a larger dataset spanning multiple sessions and participants.

Overall, no significant divergence was observed between the RTA and RSA results across the 750 NSD stimulus conditions. However, even with this limited subset of data, RTA demonstrates its potential to uncover an additional layer of structure in complex neural patterns. With future extensions to all 40 sessions and eventually all 8 subjects, RTA has the potential to yield converging results and reveal deeper insights that remain hidden beneath traditional analyses.

Discussion

While initial results do suggest that RTA's capability to reveal richer and more interesting topological structures in the neural data, the interpretation of these topological features remains a central challenge. Even when persistent homology identifies robust topological patterns (e.g. loops or connected components), the actual semantic implications or significance of these structures are often upon subjective interpretations which can be ambiguous or biased. This subjectivity limits the utility of RTA as a stand-alone method for understanding neural representations in a solid way.

To address this, future work must not only scale up in terms of data—incorporating more sessions and participants to improve robustness and generalizability—but also integrate systematic approaches to decode the stimulus properties that underlie each topological feature. Dimensionality reduction techniques like PCA or t-SNE could help reveal shared visual components among images contributing to a given topological pattern. More critically, machine learning techniques—such as unsupervised clustering or supervised classification—could be used to test whether topological features correspond to meaningful stimulus categories or perceptual dimensions.

Ultimately, if RTA is to move beyond exploratory analysis and become a reliable tool in cognitive neuroscience, it must be paired with quantitative frameworks that objectively validate its outputs. By combining RTA with machine learning and modern computational vision tools, we can begin to systematically map the abstract topological features of brain activity onto the concrete visual and semantic features in the visual world.

REFERENCES

Allen, E., St-Yves, G., Wu, Y., & al., e. (2022). A massive 7T fMRI dataset to bridge cognitive neuroscience and artificial intelligence. *Nat Neurosci 25*, 116–126.

Atlases — neuroimaging core 0.1.1 documentation. (n.d.). (n.d.). *Retrieved from https://neuroimaging-core-docs.readthedocs.io/en/latest/pages/atlases.html#id4*.

Brown, S., & Farivar, D. R. (2025, January 20). *Machine Learning and Inference for Topological Data Analysis*. Retrieved from https://cran.r-project.org/web/packages/TDApplied/vignettes/ML_and_Inference.html

Brown, S., & Farivar, R. (2024). The Topology of Representational Geometry. *bioRxiv 2024-02*.

Chazal, F., Glisse, M., Labruère, C., & Michel, B. (2014). Convergence rates for persistence diagram estimation in Topological Data Analysis. *PMLR*.

Chen, X., Martin, R., & Fischer-Baum, S. (2021). Challenges for using Representational Similarity Analysis to Infer Cognitive Processes. *A Demonstration from Interactive Activation Models of Word Reading*.

Curto, C. (2016). What can topology tell us about the neural code? *arXiv.org.* .

David, & Gallant. (2005). Predicting neuronal responses during natural vision. *National Library of Medicine*.

Drucker, D. M., & Aguirre, G. K. (2009). Different spatial scales of object similarity representation in lateral and ventral LOC. *Cereb Cortex*, 2269-2280.

Dujmovi ́c, M., Bowers, J., Adolfi, F., & Malhotra, G. (2022). The pitfalls of measuring representational similarity using representational similarity analysis. *bioRxiv 1*.

Edelman, S. (1998). Representation is representation of similarities. *Behav. Brain Sci. 21*, 449–498.

Edelsbrunner, N., Letscher, N., & Zomorodian, N. (2002). Topological persistence and simplification. *Discrete & Computational Geometry, 28(4)*, 511–533.

Koch, C. (1999). Biophysics of Computation: Information Processing in Single Neurons. *Oxford University Press*.

Kriegeskorte, N., Mur, M., & Bandettini, P. (2008). Representational similarity analysis - connecting the branches of systems neuroscience. *System Neuroscience*.

Kriegeskorte, N., Mur, M., Ruff, D. A., Kiani, R., Bodurka, J., Esteky, H., . . . Bandettini, P. A. (2008). Matching categorical object representations in inferior temporal cortex of man and monkey. *Neuron*, 1126-1141.

Rieke, F., Warland, D., De Ruyter van Steveninck, R., & Bialek, W. (1999). Spikes: Exploring the Neural Code. *Cambridge, MA, MIT Press*.

Shepard, R. N., & Chipman, S. (1970). Second-order isomorphism of internal representations: Shapes of states. *Cognitive Psychology*, 1-17.

Shepard, R. N., & Chipman, S. (1970). Second-order isomorphism of internal representations: Shapes of states. *Cognitive Psychology*, 1–17.

Singh, G., & al., e. (2008). Topological analysis of population activity in visual cortex. *J. vision 8*, 1–18.

Yamins, D. L., & DiCarlo, J. J. (2016). Using goal-driven deep learning models to understand sensory cortex. *Nature Neuroscience, 19(3)*, 356–365.

Zhang, A., & Farivar, R. (2020). Intersubject Spatial Pattern Correlations During Movie Viewing Are Stimulus-Driven and Nonuniform Across the Cortex. *Cereb Cortex Commun*.